ON THE MERGING OF TURBULENT SPOTS IN A SUPERSONIC BOUNDARY-LAYER FLOW

L. Krishnan and N D Sandham
Aeronautics and Astronautics, School of Engineering Sciences
University of Southampton
Southampton, United Kingdom
krishnan@soton.ac.uk

ABSTRACT

The complex transition flow physics associated with the merging of turbulent spots in a Mach 2 boundary-layer has been studied using direct numerical simulation (DNS). Dynamics of an isolated turbulent spot, merging of laterally displaced spots and merging of two spots in tandem are considered. The coherent structures associated with the wingtip region of the spot are found to play a major role in destabilising the surrounding laminar fluid. In the merging of laterally displaced spots a strong velocity-defect, resulting in unstable inflectional velocity profiles, is observed in the interaction zone. These local inflectional instabilities within the interaction region triggered new large scale coherent structures. During the inline merging, the calmed region behind the tail of the downstream spot is found to supress the growth of the upstream spot. The upstream spot is ultimately engulfed by the downstream spot.

INTRODUCTION

The growth and breakdown of disturbances initiates laminar-to-turbulent transition. Large amplitude disturbances can bypass the initial linear growth stage and directly enter the nonlinear growth phase. Finally, the disturbances breakdown into intermittent turbulent regions in an otherwise laminar flow. Emmons (1951) named these localised islands of turbulence as 'turbulent spots'. The growth and the merger of these turbulent spots leads to fully developed turbulent flow. The length of the transition region mainly depends on spot characteristics such as the convective speed of the leading and trailing edges of the spot, lateral growth rate and interactions between spots. A schematic of a turbulent spot is depicted in Figure.1.a.

Narasimha (1985) reviewed the transition process and turbulent spots in a variety of flows. A classical spot photograph (Figure.1.b) of Cantwell *et al.*(1978) reveals the sublayer streaky structures trailing the rear interface of the spot. To date, these streaky structures were identified only in the incompressible flow visualisation studies.Earlier, from his experimental results, Elder (1960) showed that a spot can be successfully triggered if the perturbation amplitude exceeds a critical intensity about 0.2 times the free-stream velocity. He also suggested that the region of turbulent flow is the sum of the areas of individual turbulent spots. This simple superposition is possible only if the spots grow independent of each other. Savas and Coles (1985) constructed a synthetic turbulent boundary layer by triggering an array of spots in a hexagonal pattern. They suggested that the dynamics of the spot interactions are important and questioned the simple superposition of spot areas. Moreover, the recent experiments by Makita and Nishizawa (2001) showed a stronger velocity-defect in the interaction zone and that the spot merging process is different from the simple superposition of spots. Gutmark and Blackwelder (1987) studied the inline merging of spots in an incompressible flow. They observed the celerity of the upstream spot to decrease in the calmed region of the downstream spot. Zilberman *et al.* (1977) initiated a turbulent spot in a laminar boundary layer and allowed it to interact with a turbulent boundary layer downstream. They noticed large scale structures evolving from the interactions and also found a drastic reduction in the lateral and streamwise growth of the spot.

Most of the studies to date have been performed to explore the dynamics of spots in an incompressible flow. The physics associated with the spot spreading mechanism and the spot interactions are only vaguely described in the literature. A clear understanding of the transition physics is required for the design of supersonic and hypersonic vehicles, yet data for compressible spots in the literature is very limited.

Krishnan and Sandham (2004.a) numerically showed that an increase in the Reynolds number has a destabilising effect while the Mach number inhibits the growth of a single hairpin structure into a turbulent spot in a plane Poiseuille flow. The effect of compressibility on the spreading of isolated turbulent spots in a compressible boundary layer was reported by Krishnan and Sandham (2004.b). They found a marked reduction in the lateral half-spreading of the spots from 5° to 1.7° with the flow Mach number varying from 2 to 6. Their spot substructures clearly revealed that a spot is an array of hairpin and quasi streamwise vortices. They also observed spanwise-coherent structures which are representative of the supersonic modes (Mack mode) under the front overhang of the spot in a Mach 6 boundary layer. Krishnan and Sandham (2004.c) investigated the complex flow physics associated with the interaction of a turbulent spot with an oblique shock-induced laminar separation bubble. The passage of the spot completely collapsed the bubble through a 'tunnelling' effect and the lateral half-spreading angle increased about three times that of an isolated spot.

Previous experimental results were based on ensemble-averaged flow measurements and planar visualisation images. A complete picture of the flow field can be obtained using direct numerical simulation technique, which may facilitate the interpretation of the complex three dimensional structure of a spot. The present computation is primarily carried out to improve our understanding of the physics associated with

the merging of turbulent spots in a supersonic boundary layer flow.

SPOT SIMULATIONS

Numerical Approach

The non-dimensional Navier-Stokes (N-S) equations that govern the unsteady, compressible flows in cartesian coordinates are

$$\frac{\partial \rho}{\partial t} + \frac{\partial \rho u_j}{\partial x_j} = 0 \tag{1}$$

$$\frac{\partial \rho u_i}{\partial t} + \frac{\partial \rho u_i u_j}{\partial x_j} = -\frac{\partial p}{\partial x_i} + \frac{\partial \tau_{ij}}{Re \partial x_j} \tag{2}$$

$$\frac{\partial E}{\partial t} + \frac{\partial (E+p)u_j}{\partial x_j} = \frac{\partial u_i \tau_{ij}}{\partial x_j} - \frac{1}{(\gamma-1)RePrM^2}\frac{\partial}{\partial x_j}(\mu \frac{\partial T}{\partial x_j}) \tag{3}$$

where

$$\tau_{ij} = \mu(\frac{\partial u_j}{\partial x_i} + \frac{\partial u_i}{\partial x_j} - \frac{2}{3}\delta_{ij}\frac{\partial u_k}{\partial x_k}) \tag{4}$$

The temperature is given by

$$T = \gamma(\gamma-1)M^2(E - \frac{1}{2}\rho u_i u_i) \tag{5}$$

The equation of state can be written as

$$p = (\gamma-1)(E - \frac{1}{2}\rho u_i u_i) = \frac{1}{\gamma M^2}\rho T \tag{6}$$

The non-dimensional parameters governing the flow are Reynolds number; $Re = \frac{\rho_r^* u_r^* x_r^*}{\mu_r^*}$, Mach number; $M = \frac{u_r^*}{\sqrt{\gamma R^* T_r^*}}$, ratio of specific heats; $\gamma = \frac{c_p}{c_v}$, and Prandtl number; $Pr = \frac{\mu_r^* c_p^*}{k^*}$ which is set to 0.72. The variation of the dynamic viscosity with temperature is accounted for by using a power law ($\frac{\mu^*}{\mu_r^*} = (\frac{T^*}{T_r^*})^\omega$) with a constant ω. In the above expressions the subscript r denotes a reference value and asterisks (*) represents dimensional variables.

Entropy-Splitting

The governing equations are solved using a stable high-order scheme that is free from upwinding and any other explicit artificial dissipation terms. An entropy splitting approach is used to split the Euler terms into conservative and non-conservative parts. Consider a system of hyperbolic conservation equations of the form

$$u_t + f_x = 0 \tag{7}$$

where u and f are column vectors. Applying the entropy variable transformation using the split high-order entropy conserving scheme of Girristen and Olsson (1998) gives

$$u_w w_t + f_w w_x = 0 \tag{8}$$

The final split form can be written as

$$\frac{\beta}{\beta+1}u_t + \frac{1}{\beta+1}u_w w_t + \frac{\beta}{\beta+1}f_x + \frac{1}{\beta+1}f_w w_x = 0; \beta \neq -1 \tag{9}$$

Table 1: Details of spot simulations

$M_\infty = 2.0, Re_{\delta^*_{in}} = 950.0, T_w = 1.672 T_\infty$

Case	$(L_x, L_y, L_z)/\delta^*_{in}$	N_x, N_y, N_z
Single (M2I)	400 x 60 x 60	801 x 101 x 121
Lateral (M2LM)	400 x 60 x 100	801 x 101 x 201
Tandem (M2TM)	400 x 60 x 60	801 x 101 x 121

where β is a splitting parameter. The original un-split conservative form can be recovered as $\beta \to \infty$. In the present simulation the value of β was set to 4.0 (Sandham *et al.*, 2002). All the spatial discretizations are carried out using a fourth-order central-difference scheme while the time integration uses a third-order Runge-Kutta method. A stable boundary scheme of Carpenter *et al.* (1999), along with a Laplacian formulation of the viscous and heat conduction terms, are used to prevent the odd-even decoupling associated with central schemes. An artificial compression method (ACM) variant of a standard total variation diminishing (TVD) family is used to capture flow discontinuities. The TVD filter is applied at the end of each full time step in the form of an additional numerical flux term

$$F_{j+\frac{1}{2}} = R_{j+\frac{1}{2}}\Phi_{j+\frac{1}{2}}\Psi_{j+\frac{1}{2}} \tag{10}$$

where R is the right eigenvector matrix of the flux Jacobian from the Euler equations and Φ is defined by the TVD scheme. Ψ is the sensor (Ducros *et al.*,1999) which takes low values where the flow is turbulent and values close to one in the vicinity of a shock.

$$\Psi = \frac{(div(V))_2}{(div(V))_2 + (rot(V))_2 + \epsilon} \tag{11}$$

where V is the velocity vector and ϵ is machine zero.

More details regarding the entropy-splitting and other numerical issues used in the present scheme can be found in Sandham *et al.* (2002).

Flow Details

All lengths are normalised with the displacement thickness (δ^*_{in}) of the laminar inflow profile. The laminar base flow is obtained by a separate self-similar compressible boundary layer solution. Details of the various test cases considered are given in Table.1. For the present flow conditions an unperturbed laminar base flow remained laminar. The flow domain is discretized using an equally spaced grid along the streamwise (x) and spanwise (z) directions and a stretched grid in the wall normal (y) direction. In the supersonic part of the inflow boundary all the properties are fixed, while in the subsonic region the pressure is extrapolated from the interior. Characteristic non-reflective conditions at the outlet, integrated characteristic boundary condition at the top surface and a no-slip, isothermal condition at the flat plate surface are imposed as boundary conditions. Periodic boundary conditions are applied in the spanwise direction. The variation of the dynamic viscosity with temperature is included by using a power law with an exponent value 2/3. First the laminar base flow is allowed to develop along the plate until steady-state conditions are reached. The spatially developed laminar base flow is perturbed by a localised blowing through the flat plate surface. A spanwise symmetric rectangular slot of dimensions 4 x

4 (x, z) is used. The blowing trip is activated for a short duration of 8 non-dimensional time units (δ^*_{in}/u_∞) by specifying vertical velocity at the plate surface as

$$v_{inj} = 0.2u_\infty \text{ for } \begin{cases} 20 \le x \le 24, 28 \le z \le 32, t < 8 \text{ (M2I)} \\ 36 \le z \le 40; 60 \le z \le 64, t < 8 \text{(M2LM)} \\ 28 \le z \le 32; t < 8, 98 < t < 106 \text{ (M2TM)} \end{cases}$$

The amplitude of the disturbance is chosen such that a spot can be triggered (Elder, 1960) and tracked within the present domain size.

RESULTS AND DISCUSSIONS

In this section the results for a single turbulent spot are summarized first and then the dynamics of spot merging are discussed in detail.

Single spot dynamics

Coherent structures in the flow are identified by calculating the second invariant ($\Pi = \frac{\partial u_i}{\partial x_j} * \frac{\partial u_j}{\partial x_i}$) of the velocity gradient tensor. Negative values of Π correspond to regions in the flow where the vorticity dominates over strain. The injected low momentum fluid acts as a blockage to the flow and induces hairpin vortices downstream of the injection slot. These primary hairpin structures are stretched by the mean flow shearing action and are convected downstream (Figure.2). The strength of these primary structures is high due to the large amplitude blowing trip and they trigger second-generation hairpin structures and quasi-streamwise vortices and other auxiliary structures in the flow by a vortex regeneration mechanism (Haidari and Smith, 1994). As they are convected downstream, the structures grow and their interaction finally evolves into a localised turbulent patch i.e. a turbulent spot. A turbulent spot at time t=391 (Figure.3) shows the arrowhead shaped front overhang, lateral wingtips and the longitudinal vortices around the tail interface. This looks similar to the classical spot sub-layer flow visualisation pictures of Cantwell *et al.* (1978) (Figure.1.b).

In our isolated spot results (Krishnan and Sandham, 2004.b), we noticed that the spanwise extremities at the rear of the spot (lateral wingtips) are attended by velocity-defect regions. These velocity-defect regions are caused by the upwash of near-wall fluid by coherent structures in the wingtip region. The high momentum turbulent fluid inside the spot is surrounded by the low speed laminar fluid. This creates a lateral shear along the wingtips. The rollers induced by the lateral shear are stretched in the streamwise direction by the mean shear and these structures caused the upwash of the near-wall fluid. A detailed schematic of the proposed destabilising mechanism responsible for the lateral spreading of the spot is explained in Figure.4.

This mechanism based on lateral shear explains the qualitative variation in spot spreading rate in a variety of flows, such as inhibition of the lateral growth of spots in a boundary layer with a favourable pressure gradient, enhanced growth in an adverse pressure gradient flow, suppression of the spot growth during the interaction with a turbulent boundary layer and the effects of compressibility.

The lateral half-spreading angle of the spot in the present Mach 2 flow is estimated as 5°. The spreading angle of an incompressible spots is around $8.5-11°$. The front of the spot is convected around $0.87u_\infty$ and the tail convective speed is found to be $0.53u_\infty$. The corresponding front and tail speeds of the incompressible spots reported in the literature are $0.85-0.9$ and $0.5-0.6$, respectively.

Lateral merging

Figure.5 shows a three-dimensional view of the spots during an early stage of the merging process. The spot substructures, an array of hairpin-shaped and quasi streamwise vortices, are identified inside the spot. Iso-surfaces of the streamwise velocity perturbations (relative to the laminar profile: $u' = u - u_l$) indicate a strong velocity-defect in the interaction region (Figure.6). The upwash near the interacting wingtips is stronger in comparison to the free wingtips (non-interacting)(Figure.7.a) This triggers highly unstable inflectional velocity profiles away from the wall (Figure.7.b). A schematic of the lateral merging of spots is shown in Figure.8. This inflectional instability generates new spanwise-coherent structures which later connects the longitudinal vortices along the wingtips. Thus new hairpin structures are generated in the merged region (Figure.9).

Intermittency distribution

The fraction of time a point in the surface experiences turbulent motion due to the passage of a turbulent spot can be quantitatively described using the intermittency data (γ). Dhawan and Narasimha (1958) successfully calculated the local skin friction distribution during transition (c_{ft})using intermittency data. They assumed that the skin friction during transition can be represented as a linear combination of the corresponding laminar(c_{fl}) and the turbulent skin friction (c_{fT}) values.

$$c_{ft} = (1 - \gamma)c_{fl} + \gamma c_{fT} \tag{12}$$

From the DNS results we know the laminar skin friction distribution and the transitional skin friction value. The turbulent skin friction value is obtained using the Eckert's correlation based on the reference temperature method.

$$c_{fT} = \frac{0.370}{[\log_{10}(Rex/(\rho^R\mu^R)]^{2.584}}, c_{fl} = \frac{0.664}{\sqrt{(Rex/(\rho^R\mu^R)}} \tag{13}$$

A reference temperature: $T^R = T_e + 0.5(T_w - T_e) + 0.22(T_{rec} - T_e)$ is used to caluclate the density (ρ^R) and the viscosity (μ^R) used in the correlations. T_{rec} is the adiabatic recovery temperature, T_e is the temperature at the outer edge of the boundary layer and T_w is the temperature at the wall. Comparison of the present laminar skin friction value with the Eckert's laminar correlation showed excellent agreement. The local intermittency distribution of the spot is estimated using equation.12. The intermittency distribution at the flatplate surface at time t=290 and t=396 are plotted in Figure.10. Higher values of γ are seen near the free wingtips and the interaction region. This reflects the high skin friction associated with the newly generated turbulence. The complex interaction dynamics of the spots should be taken into account for the development of accurate intermittency based transition models capable of predicting transitional flow properties.

Tandem merging

Iso-contour of the streamwise velocity perturbations at a non-dimensional time t=134 plotted in Figure.11. It shows the upstream spot entering the calmed region of the downstream spot. Further downstream the overhang region of the

upstream spot overtakes the tail of the downstream spot. The leading edge primary hairpin structure of the upstream spot can still be identified in the merged region (Figure.12). The the intermittency distribution (Figure.13) confirms the suppressed growth of the upstream spot. Due to the interaction the celerity of the downstream spot was not altered. However, the influence of its calmed region on the dynamics of the upstream spot is significant.

SUMMARY

The dynamics of an isolated turbulent spot, lateral and tandem merging of spots in a supersonic boundary layer have been studied in detail.

- An array of hairpin-shaped and quasi streamwise vortices are identified as the main spot substructures. The coherent structures in the wingtip region destabilise the surrounding laminar fluid by displacing the near-wall fluid away from the surface (upwash) and were found to be responsible for the lateral growth of the spot.

- In the lateral merging of spots a strong velocity-defect region is created in the interaction zone due to the upwash associated with the wingtip structures. The inflectional velocity profiles associated with the velocity-defect triggered new large scale structures in the interaction zone.

- The growth of a spot was highly suppressed in the re-laid laminar boundary layer (calmed region) after the passage of a downstream spot.

ACKNOWLEDGEMENTS

The authors would like to acknowledge the financial support of the European Space Agency (ESTEC) for this work.

REFERENCES

Cantwell, B and Coles, D and Dimotakis, P, 1978, Structure and entrainment in the plane of symmetry of a turbulent spot, *J. Fluid. Mech.*, 87, 641-672.

Carpenter, M.H, Nordstrom, J. and Gottlieb, D, 1999, A stable and conservative interface treatment of arbitrary spatial accuracy, *J. Comp. Phys.* **148**, 341-365.

Dhawan, S and Narasimha, R ,1958, Some properties of boundary layer flow during transition from laminar to turbulent motion, *J. Fluid. Mech.*, 3, 418-436.

Ducros, F, Ferrand, V, Nicoud, F, Weber, C, Darracq, D, Gacherieu, C and Poinsot, T, 1999, Large-Eddy simulation of the shock/turbulence interaction, *J. Comp. Phys.* **152**, 517-549.

Eckert, E.R.G, 1955, Engineering relations for skin friction and heat transfer to surfaces in high velocity flows, *J. Aero. Sci.*, 22, 585-587.

Elder, J.W, 1960, An experimental investigation of turbulent spots and breakdown to turbulence, *J. Fluid. Mech.*, 9, 235-246.

Emmons, H.W, 1951, The laminar-turbulent transition in a boundary layer, *J. Aero. Sci.*, 18, 490-498.

Gerritsen, M and Olsson, P, 1998, Designing an efficient solution strategy for fluid flows:1.A stable high order finite difference scheme and sharp shock resolution for the Euler equations, *J. Comp. Phys.* **129**, 245-262.

Gutmark, E, and Blackwelder, R.F, 1987, On the structure of a turbulent spot in a heated laminar boundary layer, *Experiments in Fluids*, 5, 217-229.

Haidari, A H and Smith, C R, 1994, The generation and regeneration of single hairpin vortices, *J.Fluid Mech.*,(277),135-162.

Krishnan, L, and Sandham, N.D, 2004.a, Large eddy simulation of compressible turbulent spots, *Advances in Turbulence X, CIMNE, Barcelona*, 467-471.

Krishnan, L, and Sandham, N.D, 2004.b, Turbulent spots in a compressible boundary-layer flow, *IUTAM Symp. on Laminar-Turbulent Transition.*

Krishnan, L, and Sandham, N.D, 2004.c, Turbulent spot/separation bubble interactions in a spatially evolving supersonic boundary layer flow, *Enhancement of NATO Military Flight vehicle Performance by Management of Interacting Boundary Layer Transition and Separation*, RTO-MP-AVT-111, (27) 1-15.

Makita, H, and Nishizawa, A, 2001, Characteristics of internal vortical structures in a merged turbulent spot, *J. Turbulence.*, 2(12), 1-16.

Narasimha, R, 1985, The laminar-turbulent transition zone in the boundary layer, *Prog. Aero. Sci.*, 22, 81-111.

Sandham, N.D, Li, Q and Yee, H.C, 2002, Entropy splitting for higher-order numerical simulation of compressible turbulence, *J. Comp. Phys.* **178**, 307-322.

Savas, O. and Coles, D.E., 1985, Coherence measurements in synthetic turbulent boundary layers, *J. Fluid. Mech.*, 160, 421-446.

Zilberman, M, Wygnanski, I and Kaplan, R.E, 1977, Transitional boundary layer spot in a fully turbulent environment, *Phys. Fluid*, 20, S258-71.

FIGURES

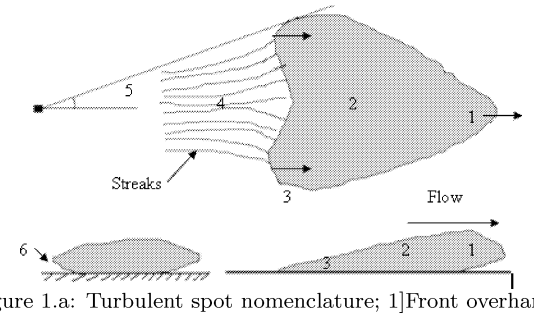

Figure 1.a: Turbulent spot nomenclature; 1]Front overhang, 2]Turbulent core, 3]Lateral wingtip, 4]Calm region, 5]Lateral spreading half-angle, 6]Spanwise overhang.

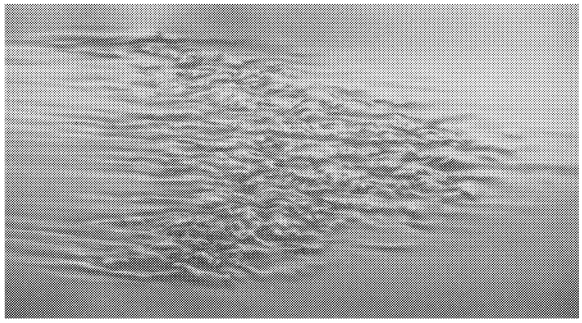

Figure 1.b: Spot flow visualisation showing the sublayer streaks (Cantwell *et al.*, 1978)

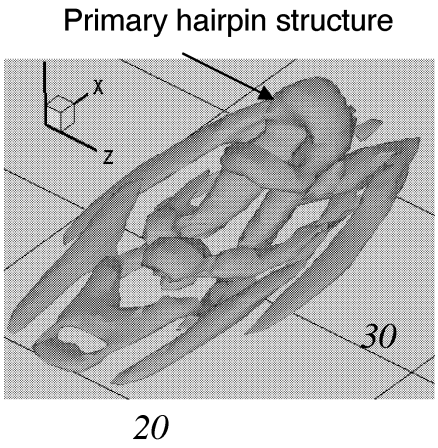

Figure 2: Coherent structures downstream of the injection slot (M2S) (t=36, Π=-0.002)

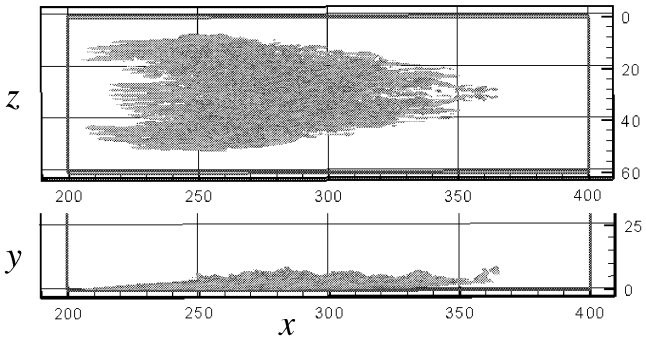

Figure 3: Top and side view of a spot (M2S) (t=391, wall-normal vorticity ω_y = +0.06,-0.06)

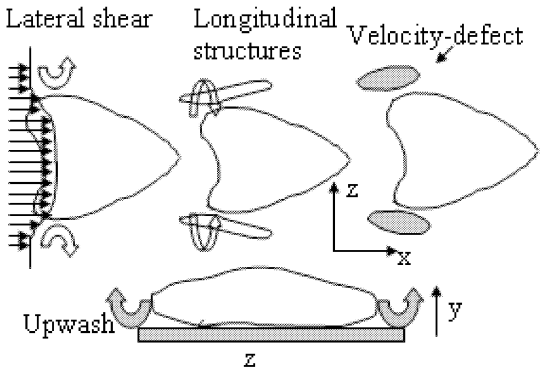

Figure 4: Proposed lateral spreading meachanism of the spot

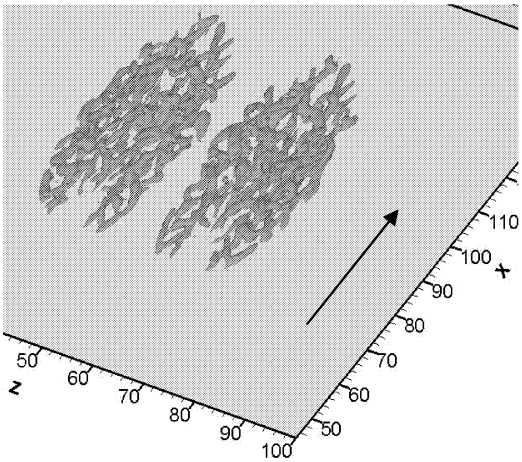

Figure 5: Lateral merging of spots (M2L) (t = 130, Π=-0.002)

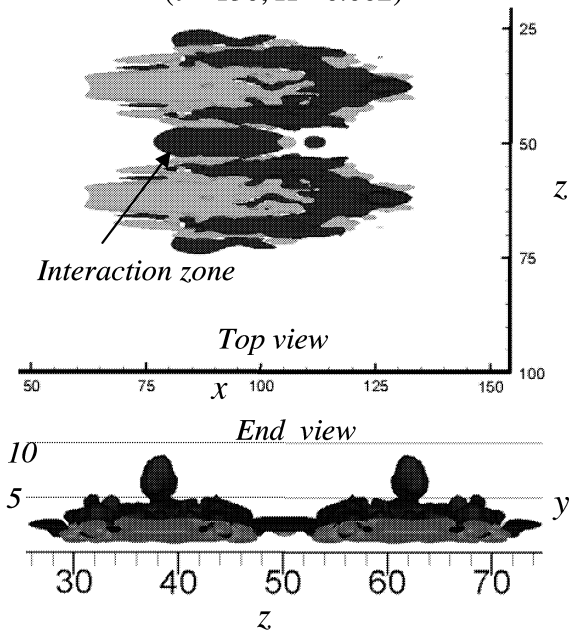

Figure 6: Streamwise velocity perturbations (M2L) (t = 130, u'=-0.02,+0.02u_∞)(Dark shade – negative value, Light shade-positive value)

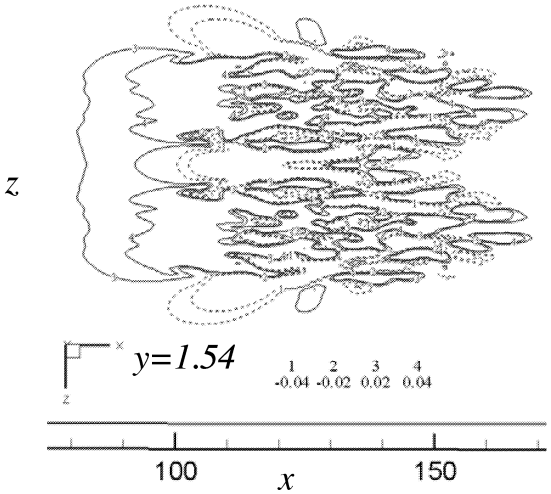

Figure 7.a: Velocity perturbations (t=173)

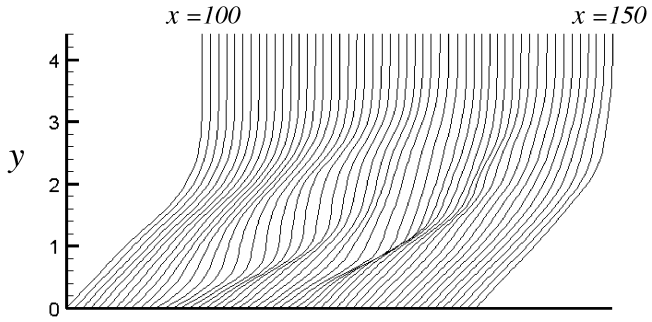

Figure 7.b: Inflectional velocity profiles in the interaction zone (M2L, t = 173, z = 50)

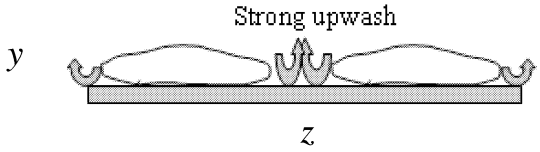

Figure 8: Outline showing the lateral interaction of spots

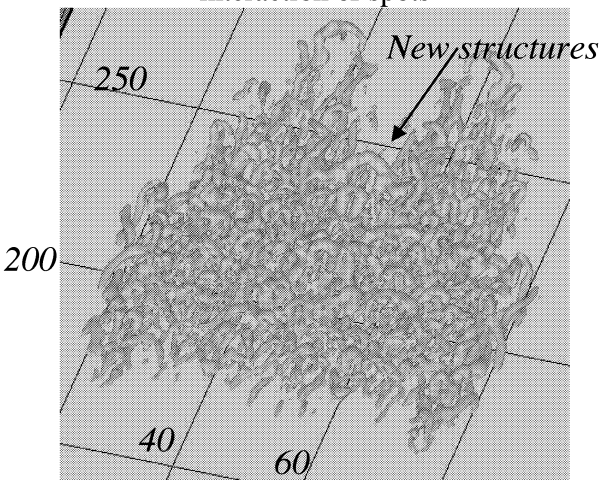

Figure 9: Coherent structures in the interaction zone (t = 290, Π= -0.002)

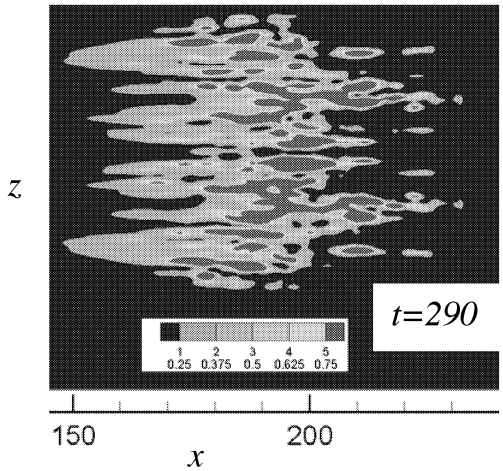

Figure 10.a: Intermittency distribution

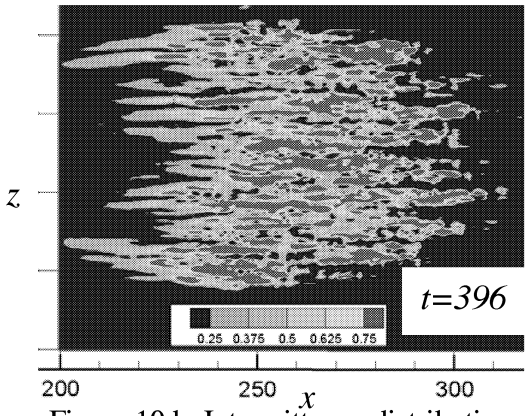

Figure 10.b: Intermittency distribution

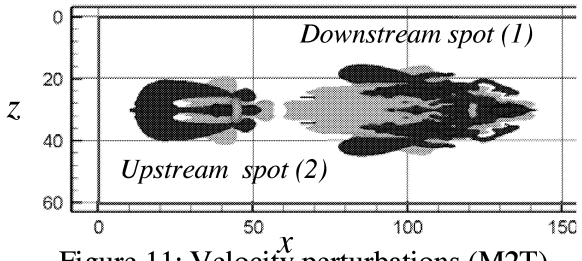

Figure 11: Velocity perturbations (M2T) (t = 134, u'=-0.02,+0.02u_∞)(Dark shade – negative value, Light shade-positive value)

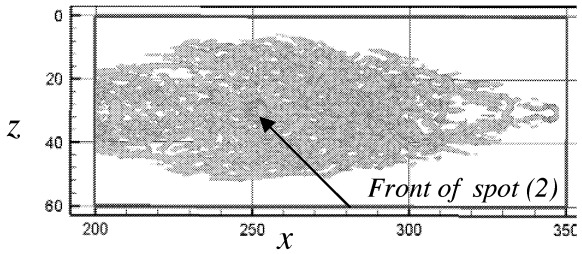

Figure 12: Coherent structures in the interaction zone (t = 374, Π= -0.002)

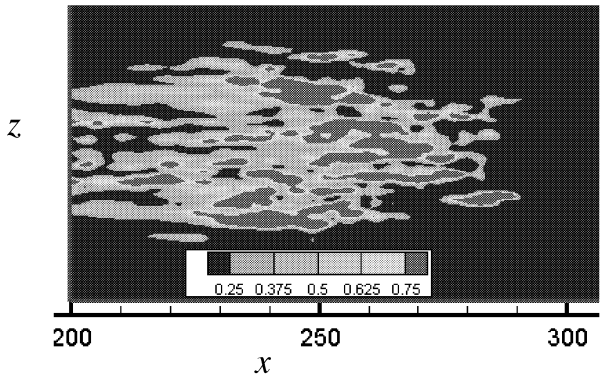

Figure 13: Intermittency distribution (t=374)